IEICE TRANS. ELECTRON., VOL.E104–C, NO.10 OCTOBER 2021

PAPER Special Section on Microwave and Millimeter-Wave Technologies

300-GHz-Band OFDM Video Transmission with CMOS TX/RX Modules and 40 dBi Cassegrain Antenna toward 6G

Yohei MORISHITA[†a)], **Sangyeop LEE**[††], ***Members***, **Toshihiro TERAOKA**[†], ***Nonmember***, **Ruibing DONG**[†††], ***Member***, **Yuichi KASHINO**[††††], **Hitoshi ASANO**[††††], ***Nonmembers***, **Shinsuke HARA**[†††], **Kyoya TAKANO**[††], **Kosuke KATAYAMA**[††], ***Members***, **Takenori SAKAMOTO**[†], **Naganori SHIRAKATA**[†], ***Nonmembers***, **Koji TAKINAMI**[†], ***Senior Member***, **Kazuaki TAKAHASHI**[†], **Akifumi KASAMATSU**[†††], **Takeshi YOSHIDA**[††], **Shuhei AMAKAWA**[††], ***Members***, ***and*** **Minoru FUJISHIMA**[††], ***Fellow***

SUMMARY This paper demonstrates 300 GHz terahertz wireless communication using CMOS transmitter (TX) and receiver (RX) modules targeting sixth-generation (6G). To extend communication distance, CMOS modules with WR-3.4 waveguide interface and a high-gain antenna of 40 dBi Cassegrain antenna are designed, achieving 36 Gbps throughput at a 1 m communication distance. Besides, in order to support orthogonal frequency-division multiplexing (OFDM), a self-heterodyne architecture is introduced, which effectively cancels the phase noise in multi-carrier modulation. As a proof-of-concept (PoC), the paper successfully demonstrates real-time video transfer at a 10 m communication distance using fifth-generation (5G) based OFDM at the 300 GHz frequency band.

key words: *6G, THz, 300 GHz, Cassegrain antenna, OFDM, CMOS, transmitter, receiver, module*

1. Introduction

5G service has begun wide deployment in 2020, where in addition to utilizing the sub-6 GHz frequency band, the millimeter-wave frequency band, typically around 28 GHz, is being introduced for enhanced Mobile Broadband (eMBB) that achieves multi-Gigabit-per-second (multi-Gbps) throughput. Recently, 5G evolution has been under discussion, and the use of the 52 GHz is being studied for further enhancement [1]. Following this trend, terahertz frequency bands, i.e., 100 GHz to 300 GHz, is also being studied toward 6G [2], [3].

By utilizing its broadband characteristic of the terahertz band which even exceeds the millimeter frequency bands, it is possible to further enhance the wide range of B2C (Business-to-Consumer)/B2B (Business-to-Business) services that will be put into practice by 5G. Typical use cases of terahertz communication are wireless backhaul/fronthaul, ultra-high-definition video transfer and bulk data upload/download, to name a few examples.

Manuscript received October 23, 2020.
Manuscript publicized January 26, 2021.
[†]The authors are with Panasonic Corporation, Yokohama-shi, 224–8539 Japan.
[††]The authors are with Hiroshima University, Higashihiroshima-shi, 739–8530 Japan.
[†††]The authors are with the National Institute of Information and Communications Technology, Koganei, Tokyo, 184–8795 Japan.
[††††]The authors are with Panasonic System Networks R&D Lab. Co., Ltd., Sendai-shi, 981–3206 Japan.
a) E-mail: morishita.yohei@jp.panasonic.com
DOI: 10.1587/transele.2021MMP0005

Realization of terahertz wireless transceivers has been actively studied in academic and research institutes, and previous works report photonic-based transceivers [4], [5] and compound semiconductor-based transceivers [6]–[8]. On the other hand, in order to introduce terahertz wireless communication into the market, suitability of mass-production is critically important. To this end, the authors have studied realization of CMOS-based 300 GHz transceivers [9]–[13] and achieved 32 Gbps throughput [12].

However, the communication distance of the previous work [12] is only 5 cm and the experiments are done with on-wafer probing. Moreover, the work demonstrated the performance of single-carrier modulation, but OFDM will likely be adopted in 6G as a natural extension of 5G. In this paper, we tackle the extension of communication distance and the support of an OFDM signal based on 5G. As a proof-of-concept, this paper also demonstrates real-time video transfer using the 300 GHz frequency band [14], [15].

The major contributions of this paper are as follows.

1. Designed 300 GHz CMOS TX/RX modules and high-gain Cassegrain antenna realizing 36 Gbps throughput at a 1 m communication distance.
2. Introduced a self-heterodyne architecture that lowers inter-carrier interference (ICI) due to phase noise, enabling OFDM communication at the 300 GHz frequency band.
3. Demonstrated real-time video transfer over a 10 m communication distance at the 300 GHz frequency band with 5G based OFDM as a PoC of 6G.

This paper is organized as follows. Section 2 addresses the issues of extending the communication distance and support of an OFDM. It also explains implementation and operation principles of two selected architectures. Section 3 describes the design of TX/RX modules and Sect. 4 covers the high-gain antenna design. Section 5 shows measurement results, and is followed by concluding remarks in Sect. 6.

2. System Architecture

This section first discusses the issues of extending the communication distance and support of an OFDM, and then introduces two selected architecture used in this paper.

Table 1 Reference of 5G based OFDM signal.

System specification	Description
Supported modulation (Codding rates)	BPSK (1/5) QPSK (1/4, 1/2, 3/4) 16-QAM (1/2, 3/4, 7/8) 64-QAM (3/4, 7/8)
Waveform (OFDM)	2048 FFT size, 160/144 CP length, 1200 active subcarriers, 75-kHz subcarrier spacing
Bandwidth	N×100 MHz component carriers (N = 8 max)
Component carrier spacing	100 MHz
Occupied bandwidth	90.075 MHz

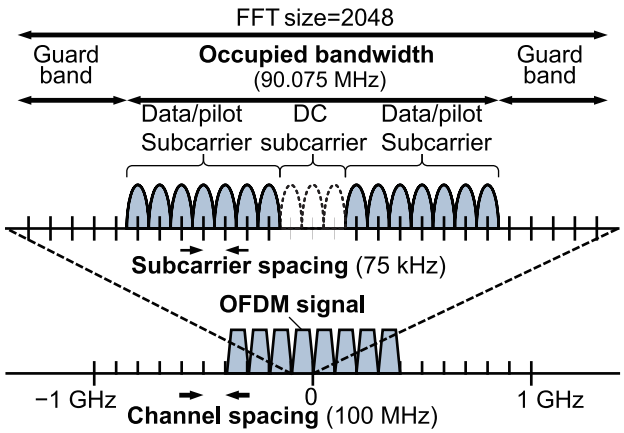

Fig. 1 Spectrum of 5G based OFDM signal.

2.1 Issues of Extending the Communication Distance

Assuming an in-studio use-case with 10 m wireless communication such as video transmission from TV cameras, the free space loss at 300 GHz is more than 100 dB. In order to extend the communication distance, high transmission power, low noise figure (NF) and high antenna gain are required. However, since the maximum operating frequency ($f_{\max}$) of CMOS technology is comparable to or lower than the terahertz frequency, it is difficult to integrate RF amplifiers in CMOS technology. In addition, it is difficult to design a high gain antenna on IC or printed circuit board (PCB) because of its large loss in 300 GHz band. To extend communication distance, development of modules that can interface with an external RF amplifier or a high-gain antenna via the WR-3.4 rectangular waveguide (WG) interface is required. Moreover, the design of high gain antenna with WR-3.4 interface is required.

2.2 Issues of OFDM System

5G utilizes OFDM in its waveform that provides flexibility in the size of the spectrum allocation and the bandwidth. However, the OFDM requires lower phase noise as compared to the single-carrier modulation [16]–[18], which is critical for a terahertz frequency band because the phase noise of radios are escalated by a factor of 20 log(N) where N is the multiplication factor of a carrier frequency. Table 1 summarizes specifications of OFDM used in this paper, which are based on 5G. The FFT size is 2048 points, and it employs turbo coding as an error correction scheme. The modulation and coding scheme (MCS) can vary depending on the environment. In this work, eight OFDM signals are lined up as illustrated in Fig. 1. Since subcarrier spacing is only 75 kHz, each subcarrier suffers from ICI. The OFDM signals are greatly affected by phase noise because of the narrow subcarrier spacing.

2.3 300-GHz-Band Wireless System

In this paper, two different modes of architectures are adopted.

Figure 2 (a) shows Mode 1, which is a heterodyne architecture. TX and RX circuits are based on the ones presented in [10], [11] and external local signals (LOs) are fed to TX and RX circuits.

Figure 2 (b) shows Mode 2, which is a self-heterodyne architecture [15], [19]–[22]. In this architecture, the LO is transmitted from the TX, which is used as the LO in the RX. Since the same LOs are utilized in both TX and RX, the phase noise can be canceled. In addition, since the LO chain in the RX is not required, power consumption can be reduced.

In this paper, Mode 1 is intended for evaluating highest throughput at an extended communication distance, whereas Mode 2 is adopted to demonstrate real-time video transfer utilizing a 5G based OFDM signal.

2.4 Operation Principle

By referring to Fig. 2, operation principles of Mode 1 and Mode 2 are analyzed.

The inputs of the up-conversion mixers, IF, are multiplied by the LO_{E}^3, which is expressed as

$$IF_2 = K \cdot LO_{\mathrm{E}}^3 \cdot IF, \tag{1}$$

where K represents constant coefficient. In addition to (1), LO leakage signals, LO_{E}^3, are fed into the square mixers, and the outputs of square mixers, RF_{P} and RF_{N}, are given as follows.

$$RF_{\mathrm{P}} = A(LO_{\mathrm{E}}^3 + IF_2)^2 \tag{2}$$

$$RF_{\mathrm{N}} = B(LO_{\mathrm{E}}^3 - IF_2)^2, \tag{3}$$

where A and B represent constant coefficients. These outputs are combined by a balun. Assuming the imbalance ratio of the balun input as $\Delta\alpha$, the single-ended output, RF_{S}, is expressed as

$$\begin{aligned} RF_{\mathrm{S}} &= RF_{\mathrm{P}} - RF_{\mathrm{N}} \\ &= LO + RF + A\Delta\alpha IF_2^2, \end{aligned} \tag{4}$$

where

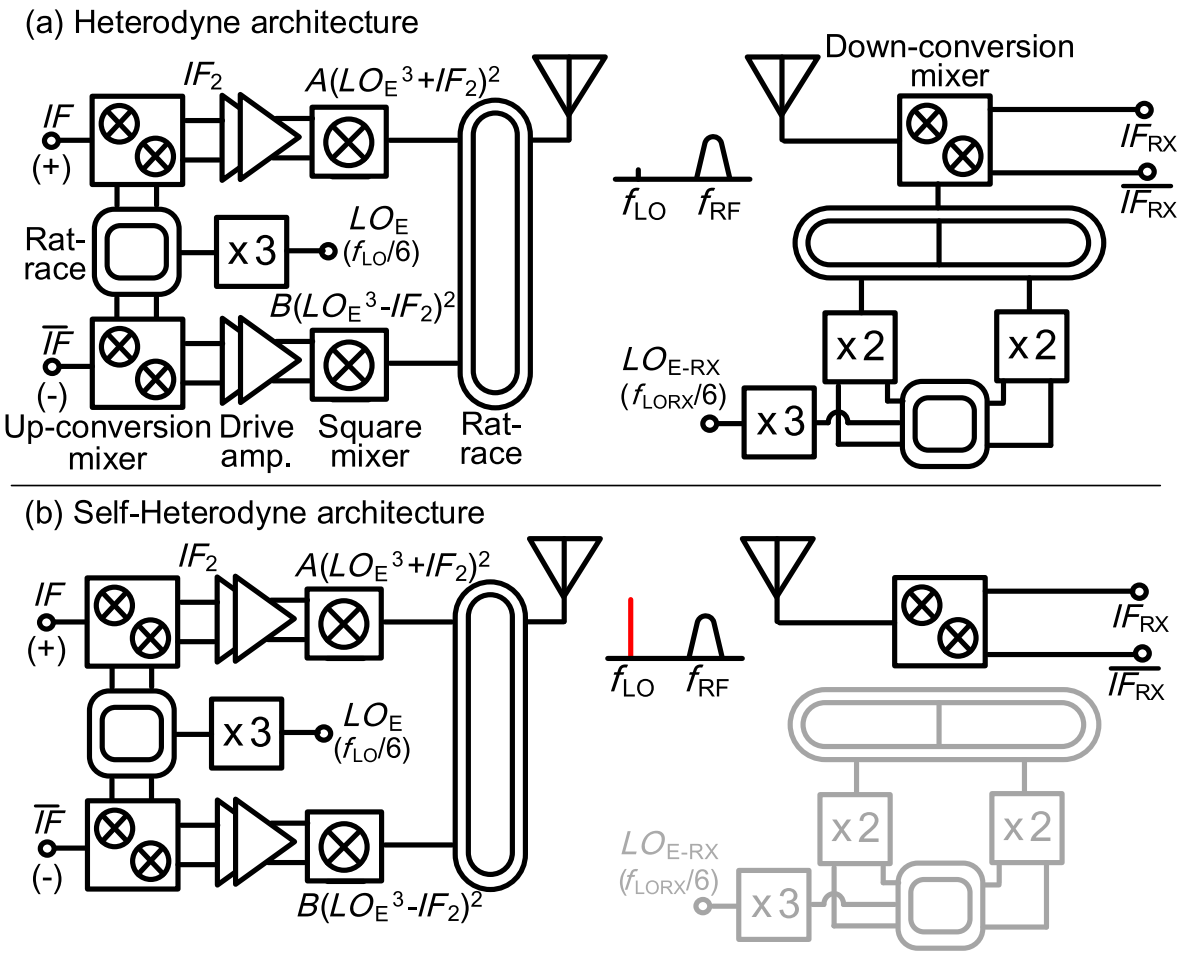

Fig. 2 Proposed architecture of 300-GHz band wireless system: (a) Heterodyne architecture (Mode 1), and (b) Self-heterodyne architecture (Mode 2).

$$LO = A\Delta\alpha LO_{\mathrm{E}}^{6} \tag{5}$$

$$RF = 2K(2-\Delta\alpha)A \cdot LO_{\mathrm{E}}^{6} \cdot IF \tag{6}$$

$$\Delta\alpha = \frac{A-B}{A}. \tag{7}$$

In Mode 1, by adjusting the bias condition of the driver amplifiers, $\Delta\alpha$ can be sufficiently made small to eliminate unwanted signal components, and then (4) is approximated as $4KA \cdot LO_{\mathrm{E}}^{6} \cdot IF$. In Mode 2, the bias condition of driver amplifiers are adjusted to create imbalance of the differential signals, and then the LO leakage, LO, as well as the desired signal, RF are transmitted from the antenna.

In the receiver side, the input RF signal is downconverted by the down conversion mixer. Since the LO is transmitted from TX in Mode 2, the LO chain does not need to operate in Mode 2. In actual implementation, the mixer in the RX is based on a double balanced mixer. In Mode 1, the LOs in the RX are input to the gate nodes of MOSFET switches. In Mode 2, both RF and LO transmitted by the TX are fed to source nodes of MOSFET switches in the RX. In this case, the mixer operates as a source pumped mixer [22].

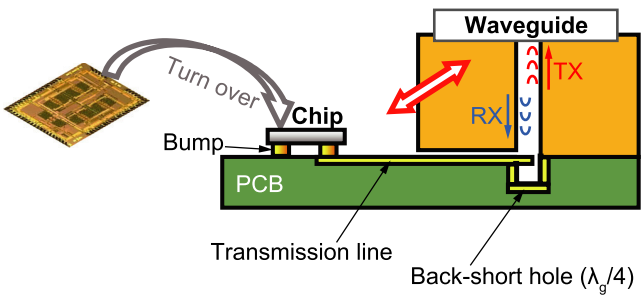

Fig. 3 CMOS-chip-to-waveguide transition via multilayer PCB.

3. Module Design

This section describes the design of TX and RX modules [23]–[26]. To extend communication distance, we develop TX/RX modules that can interface with a high-gain antenna via the WR-3.4 rectangular WG interface.

The CMOS chip is flip-chip mounted on a multilayered glass epoxy PCB, which are superior to LTCC (Low Temperature Co-fired Ceramics) boards [27] in terms of cost.

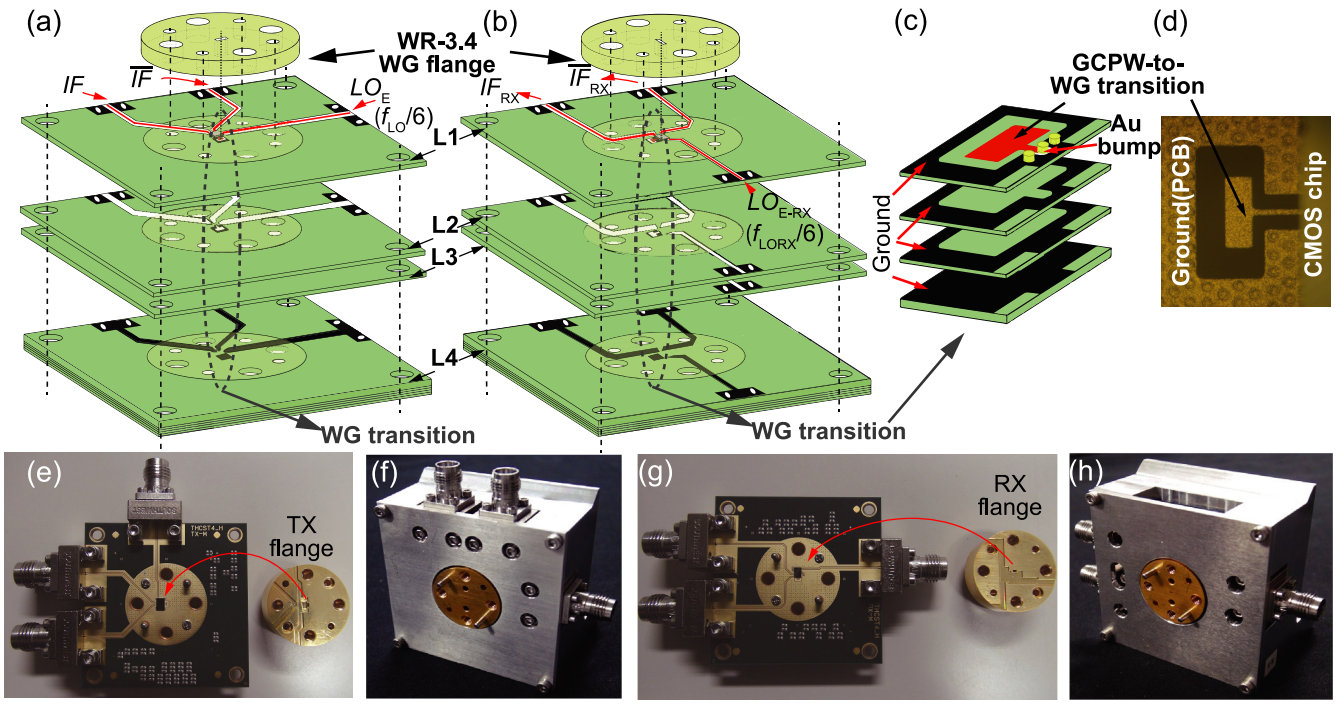

Fig. 4 Structure of the CMOS-chip-to-WG transition via multilayer PCB: (a) TX module, (b) RX module, (c) close-up of the GCPW-to-WG transition, (d) top view of the transition. And photograph of the module: (e) TX module, (f) TX module with housing, (g) RX module, and (h) RX module with housing.

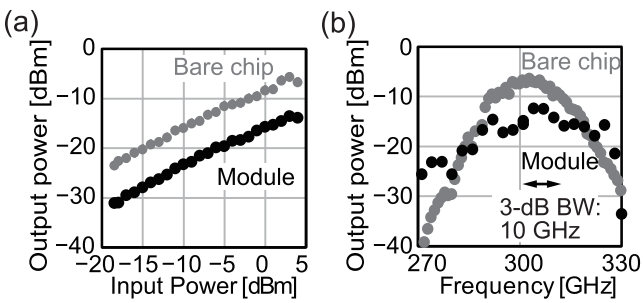

Fig. 5 Measured output power of the TX module (a) as a function of input IF power, and (b) as a function of frequency.

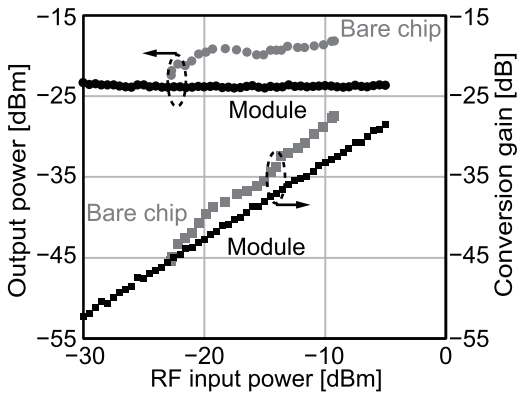

Fig. 6 Measured output power and conversion gain of the RX module and bare chip with an IF output as a function of RF input power.

In the following, the module structure and performance are briefly explained.

3.1 TX and RX Modules with CMOS-Chip-to-WG Transition

Figure 3 shows the conceptual design of our CMOS-chip to-WG transition [26]. We adopt a two-stage transition: from CMOS chip to the PCB and then from the PCB to the WG.

The designed module structure is explained with Fig. 4. Figure 4 (a) and (b) show the layers of the glass epoxy PCB of the TX module and the RX module, respectively. The CMOS TX chip [10] and the RX chip [11], fabricated using a 40 nm CMOS technology, are mounted near the center of the PCB by gold stud bump flip-chip bonding underneath a WR-3.4 waveguide flange. They are connected to a short grounded coplanar waveguide (GCPW). Figure 4 (c) shows a close-up view of the GCPW-to-rectangular-waveguide transition. The pads for the 300 GHz RF signal are 75 μm-pitch ground-signal-ground (GSG) pads. The height of the bumps is approximately 20 μm. Figure 4 (d) shows a rectangular "probe" that excites the TE10 mode in the WR-3.4 WG flange. The "probe" is made of the top metal layer (L1) of the PCB and a back-short is made of the bottom metal layer (L4). Vias, L2 and L3 layers form the vertical back-short hollow in the PCB. The depth of the back-short structure should ideally be $\lambda_g/4$, where λ_g is the wavelength of the RF signal in waveguide. Figure 4 (e) and (g) show TX and RX modules with the WR-3.4 WG flange. The WR-3.4

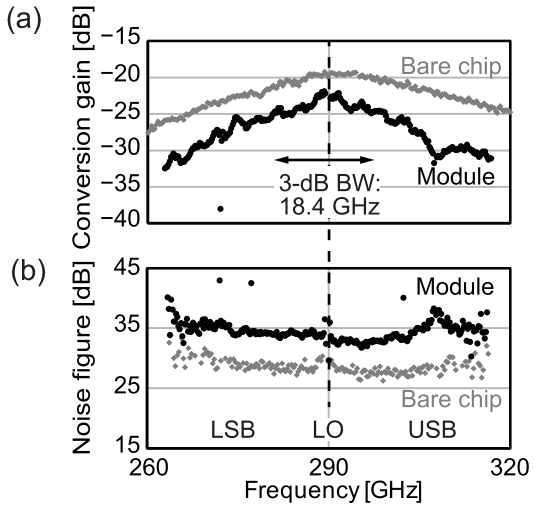

Fig. 7 (a) Measured conversion gain, and (b) noise figure of the RX module and bare chip as a function of RF frequency.

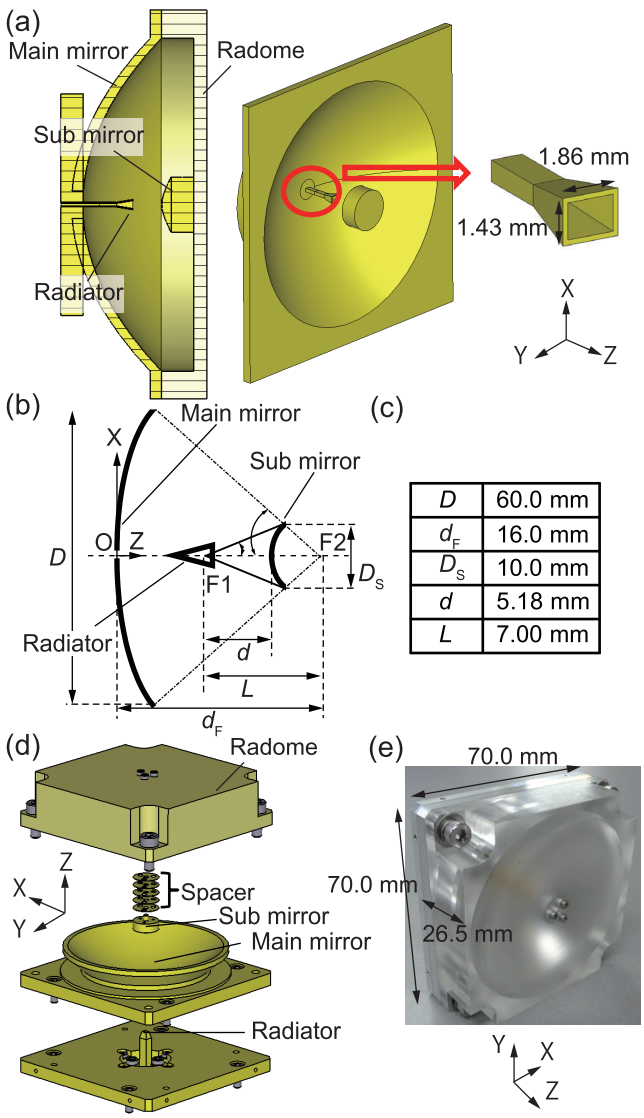

D	60.0 mm
d_F	16.0 mm
D_S	10.0 mm
d	5.18 mm
L	7.00 mm

Fig. 8 Designed Cassegrain antenna: (a) Structure, (b), (c) design parameters, (d) adjustment composition, and (e) photograph of the antenna.

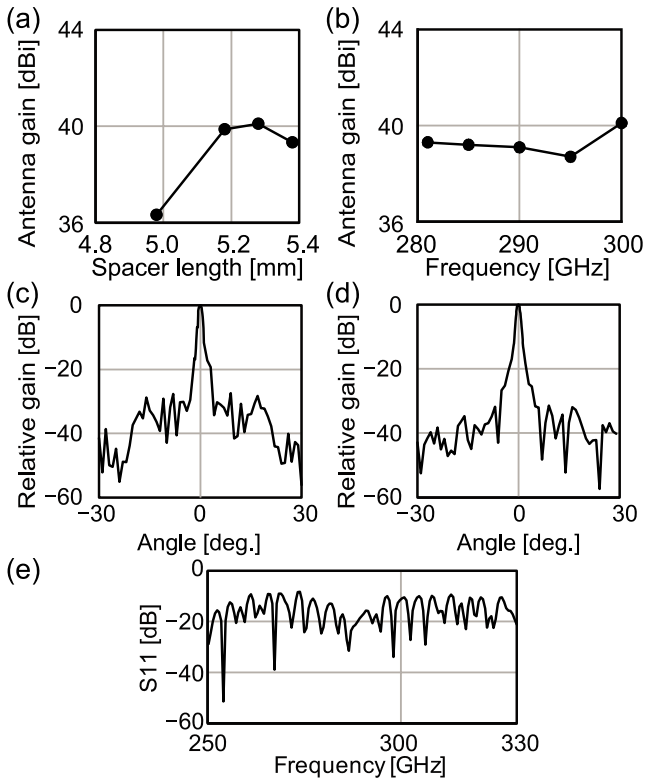

Fig. 9 Measured antenna performance: (a) Antenna gain versus spacer length, (b) frequency response. (c), (d) E-plane/H-plane directivity, and (e) return loss.

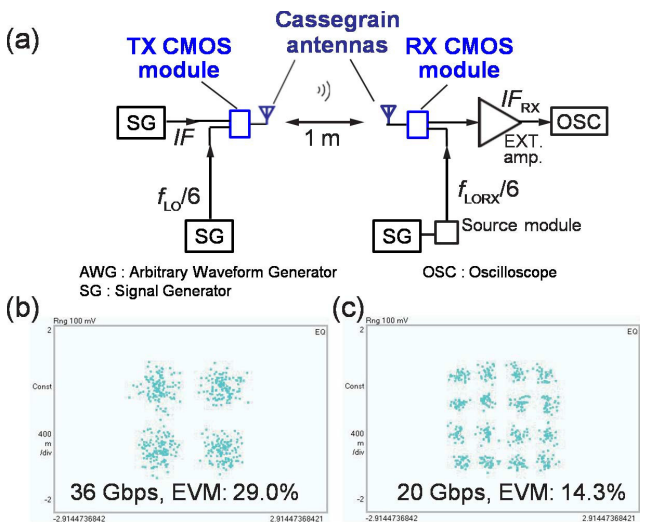

Fig. 10 (a) Measurement system of 1 m wireless transmission: f_{LO} = 280.6 GHz, f_{LORX} = 302.6 GHz, f_{IF} = 11 GHz. Measured constellations: (b) QPSK 36 Gbps, (c) 16QAM 20 Gbps.

flange mounted on the PCB completely covers the chip, the GCPW, and the back-short hollow. On the bottom side of the flange is a hollow that accommodates the chip. Figure 4 (f) and (h) show TX and RX modules with an aluminum housing.

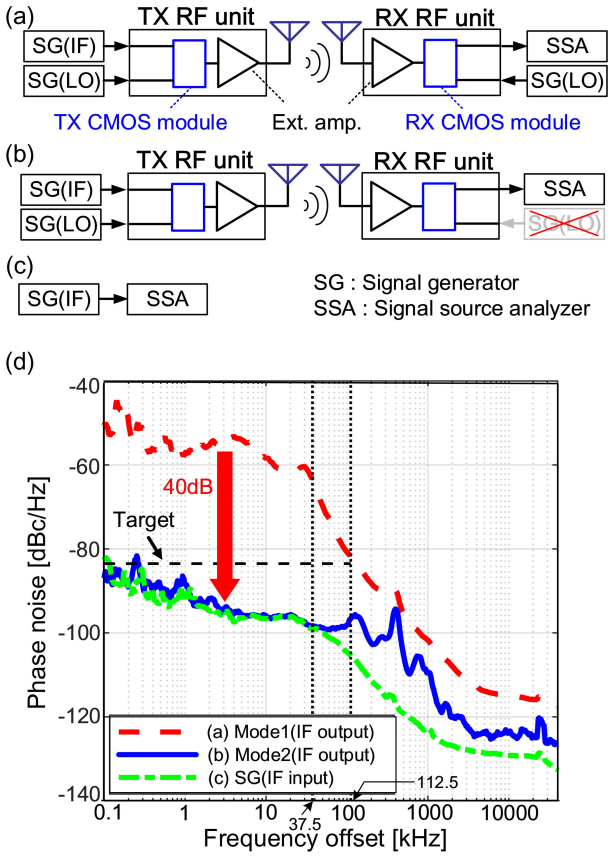

Fig. 11 Phase-noise-measurement setup: (a) IF output (Mode 1), (b) IF output (Mode 2), (c) IF input, and (d) measured results of the phase noise.

3.2 Module Performance

Figure 5 shows the measured output power of the TX module. The IF frequency and the external LO power are set to 1 GHz and 6 dBm. Figure 5 (a) shows the measured output power of the TX module as a function of the input IF power. The $f_{LO}/6$ is set to 48.5 GHz. The peak output power of the desired signal is −13.5 dBm. The peak output power of the bare CMOS chip is −5.5 dBm and the packaging loss is estimated as about 8 dB. Figure 5 (b) shows the frequency response of the output power of the TX module. The input IF power is set to 4 dBm. The 3 dB bandwidth is approximately 10 GHz with a center frequency of 305 GHz.

The measured output power and the conversion gain of the RX module in Mode 1 as a function of the input RF power are shown in Fig. 6. The RF frequency is set to 291 GHz and $f_{LORX}/6$ signal is set to 48.3 GHz with 2 dBm. The peak conversion gain is about −23.7 dB. The output power of the CMOS bare chip is −19.5 dBm, and the packaging loss is estimated as about 4 dB. Figure 7 shows the conversion gain and the NF of the RX module as a function of the input frequency. The RF input power is set to −15 dBm, and the $f_{LORX}/6$ signal is set to 48.3 GHz with 2 dBm. The 3 dB bandwidth of the module is measured as 18.4 GHz. The total NF of the RX is measured as about 33 dB, which is 6 dB higher than that of the CMOS bare chip.

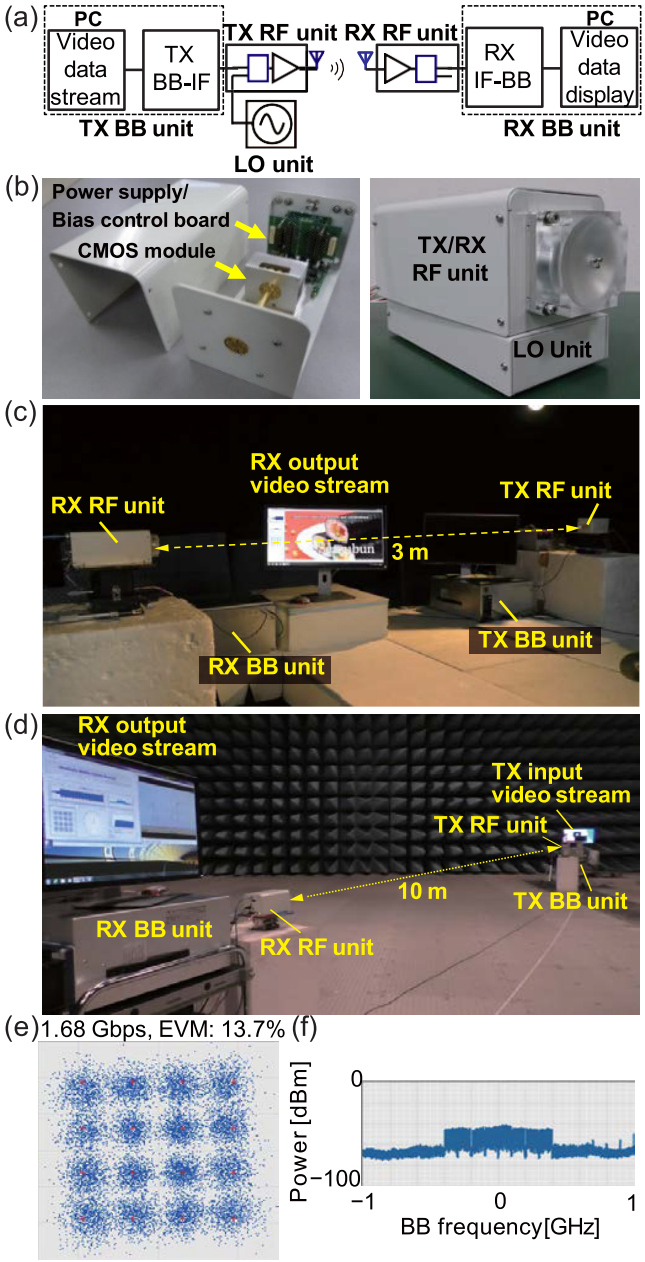

Fig. 12 300-GHz-band real time video transfer system: (a) Block diagram, (b) photograph of RF and LO unit, and measurement setup at the distance of (c) 3 m, (d) 10 m. (e) Measured constellation and spectrum at 10 m.

4. Antenna Design

This section describes design of a high-gain Cassegrain antenna with WR-3.4 WG interface [14], [28].

4.1 Antenna Structure

Figure 8 (a) shows the structure of the Cassegrain antenna. A horn antenna is used for the radiator. The main and sub

Table 2 Performance summary and comparison.

	Technology (IC)	Frequency [GHz]	Antenna gain [dBi]	Distance [m]	Data rate [Gbps]	Real-time video transfer?	Modulation
This work	40-nm CMOS w/ external amp.	293.7	39 (290GHz) 40 (300GHz)	10	1.68	Yes	OFDM (16QAM)
	40-nm CMOS	291.6	39 (290GHz) 40 (300GHz)	1	36	No	Single carrier (QPSK)
[6]	80-nm InP HEMT	290	50	9.8	120	No	Single carrier (16QAM)
[7]	35-nm GaAs mHEMT	300	24	1	64	No	Single carrier (QPSK)
[8]	35-nm GaAs mHEMT	240	55	850	64	No	Single carrier (8PSK)
[30]	130-nm SiGe	230	N. A.	1	100	No	Single carrier (16QAM)

mirrors are made of aluminum. The submirror is attached to the radome. The radome is fabricated of Cyclo-Olefin Polymer (COP). Figure 8 (b) and (c) summarize the design parameters, which are optimized for higher gain by using the finite-difference time-domain (FDTD) method. Since the wavelength of the 300 GHz signal is only 1 mm (in free space), the manufacturing error degrades the antenna performance. Simulation results indicate that the distance between the radiator and the sub mirror has large impact. To compensate for this variation, as illustrated in Fig. 8 (d), we introduce spacers between the sub mirror and the radome to adjust the distance in the manufacturing process. The manufactured Cassegrain antenna is shown in Fig. 8 (e).

4.2 Antenna Performance

Figure 9 summarizes the measured antenna performance. In Fig. 9 (a), the distance between the radiator and the sub mirror is varied by changing the number of spacers. At the optimum, more than 40 dBi maximum gain is achieved. Figure 9 (c) and (d) show the measured antenna patterns. The half width is about 1.3°. The antenna aperture efficiency is 28.1%, which is 22.6% higher than that reported in [29].

5. Wireless System Performance

In this section, we first evaluate the throughput of the CMOS modules with Cassegrain antenna. After that, we investigate effects of phase noise reduction by introducing the self-heterodyne architecture, and then demonstrate real time video transfer with 5G based OFDM signals.

5.1 Throughput of CMOS Modules with Cassegrain Antenna

Figure 10 shows the measurement setup and measured constellations of 1 m wireless transmission with employing 40 dBi Cassegrain antennas. TX/RX modules operate in Mode 1 with single carrier modulation signal in order to evaluate the highest throughput of the CMOS modules with Cassegrain antenna.

Figure 10 depicts measured constellations of the two cases. The maximum data rate of 36 Gbps with QPSK modulation is achieved at the carrier frequency of 291.6 GHz. With lower symbol rate, it can also support 16QAM at the data rate of 20 Gbps.

5.2 Phase Noise Reduction Due to Self-Heterodyne Architecture

To investigate effects of phase noise reduction due to the self-heterodyne architecture, we measured phase noise at IF output (Mode 1/Mode 2) and IF input as illustrated in Fig. 11 (a)–(c). The RF unit is composed of TX or RX CMOS module, the bias control board, the power supply board, and the external amplifier (TX: Gain 15 dB, RX: Gain 26 dB, NF 8 dB).

Figure 11 (d) shows the measured results. By comparing the phase noise of the IF outputs (Mode 1/Mode 2), we confirm that Mode 2 achieved about 40 dB lower phase noise at 10 kHz offset frequency. The IF output phase noise of Mode 2 is close to that of the IF input (SG). These results validate the effect of phase noise cancellation due to the self-heterodyne architecture. The data rate of the video source for the real time transfer is 1.68 Gbps, which requires 19 dB of CNR (Carrier-to-Noise Ratio). Assuming that the CNR degradation by phase noise is less than 0.4 dB, the integrated phase noise over the 225 kHz bandwidth, which corresponds to three subcarrier spacing, is −30 dBc. This is translated to −83.5 dBc/Hz of in-band phase noise, which is satisfied by Mode 2 as shown in Fig. 11 (d).

5.3 Real Time Video Transfer with 5G Based Protocol

To prove the concept, we demonstrate real time video transfer at a 300 GHz frequency band. Figure 12 (a) shows a block diagram of the system where TX/RX modules operate in Mode 2. PCs and the baseband (BB) units are interfaced with PCI Express. The TX BB unit generates OFDM signals shown in Fig. 1 at a 10.5 GHz IF frequency, which is up-converted to 293.7 GHz by the TX RF unit. The RF signal and TX LO leakage are transmitted and received by TX and RX Cassegrain antennas. The RX RF unit down-converts the received RF signal to a 10.5 GHz IF frequency by using received TX LO leakage, which is demodulated by the RX BB unit to stream a video on the display monitor. The hardware of the RF unit is housed in a compact case as

well as an LO unit. Figure 12 (b) shows a photograph of the system, whose volume is 15 cm×20 cm×10 cm.

Figure 12 (c) and (d) show measurement setup at 3 m and 10 m communication distance. Figure 12 (e) and (f) show the constellation and the output spectrum measured at a 10 m communication distance. Measured error-vector-magnitude (EVM) is 13.7%. As shown in Fig. 12 (d), the developed prototype system successfully demonstrates real time video transfer at a 10 m distance.

Table 2 summarizes a performance comparison. Using CMOS modules, this work achieves 36 Gbps throughput at a 1 m communication distance. In addition, this work achieves 10 m real-time video transfer with 5G based OFDM signals at a 300 GHz frequency band.

6. Conclusion

This paper has demonstrated 300 GHz terahertz wireless communication using CMOS transmitter and receiver modules. To extend communication distance, CMOS modules with WR-3.4 waveguide interface and a high-gain antenna of 40 dBi Cassegrain antenna have been designed, achieving 36 Gbps throughput at a 1 m communication distance. Besides, in order to support OFDM, a self-heterodyne architecture has been introduced, which effectively cancels the phase noise in multi-carrier modulation. As a proof-of-concept, the paper has successfully demonstrated 10 m real time video transfer using 5G based OFDM at a 300 GHz frequency band.

Acknowledgments

This work was supported by the Ministry of Internal Affairs and Communications of Japan. The authors thank J. Sato, T. Murata, and K. Mizuno for their contribution to the project.

References

[1] E. Dahlman, S. Parkvall, J. Peisa, and H. Tullberg, "5G evolution and beyond," Int. Workshop on Signal Processing Advances in Wireless Communications, pp.1–5, July 2019.
[2] M. Patzold, "5G sets sail around the globe," IEEE Veh. Technol. Mag., vol.14, no.2, pp.5–11, June 2019.
[3] NTT DOCOMO, "6G White Paper," https://www.nttdocomo.co.jp/binary/pdf/corporate/technology/whitepaper_6g/DOCOMO_6G_White_PaperJP_20200820.pdf., July 2020.
[4] G. Ducournau, P. Szriftgiser, A. Beck, D. Bacquet, F. Pavaneloo, E. Peytavit, M. Zaknoune, T. Akalin, and J.-F. Lampin, "Ultra-wide-bandwidth single-channel 0.4-THz wireless link combining broadband quasi-optic photomixer and coherent detection," IEEE Trans. Terahertz Sci. Technol., vol.4, no.3, pp.328–337, May 2014.
[5] T. Nagatsuma, Y. Fujita, Y. Yasuda, Y. Kanai, S. Hisatake, M. Fujiwara, and J. Kani, "Real-time 100-Gbit/s QPSK transmission using photonics-based 300-GHz-band wireless link," IEEE Topical Meeting on Microw. Photonics, pp.27–30, Nov. 2016.
[6] H. Hamada, T. Tsutsumi, H. Matsuzaki, T. Fujimura, I. Abdo, A. Shirane, K. Okada, G. Itami, H. Song, H. Sugiyama, and H. Nosaka, "300-GHz-Band 120-Gb/s wireless front-end based on In-P-HEMT PAs and mixers," IEEE J. Solid-State Circuits, vol.55, no.9, pp.2316–2335, Sept. 2020.
[7] I. Kallfass, I. Dan, S. Rey, P. Harati, J. Antes, A. Tessmann, S. Wagner, M. Kuri, R. Weber, H. Massler, A. Leuther, T. Merkle, and T. Kürner, "Towards MMIC-based 300 GHz indoor wireless communication systems," IEICE Trans. Electron., vol.E98-C, no.12, pp.1081–1090, Dec. 2015.
[8] I. Kallfass, F. Boes, T. Messinger, J. Antes, A. Inam, U. Lewark, A. Tessmann, and R. Henneberger, "64 Gbit/s transmission over 850 m fixed wireless link at 240 GHz carrier frequency," J. Infrared Milli. Terahz. Wave, vol.36, no.2, pp.221–233, Feb. 2015.
[9] K. Katayama, K. Takano, S. Amakawa, S. Hara, A. Kasamatsu, K. Mizuno, K. Takahashi, T. Yoshida, and M. Fujishima, "A 300 GHz CMOS transmitter with 32-QAM 17.5 Gb/s/ch capability over six channels," IEEE J. Solid-State Circuits, vol.51, no.12, pp.3037–3048, Dec. 2016.
[10] K. Takano, S. Amakawa, K. Katayama, S. Hara, R. Dong, A. Kasamatsu, I. Hosako, K. Mizuno, K. Takahashi, T. Yoshida, and M. Fujishima, "A 105 Gb/s 300 GHz CMOS transmitter," Int. Solid-State Circuits Conf., pp.308–309, Feb. 2017.
[11] S. Hara, K. Katayama, K. Takano, R. Dong, I. Watanabe, N. Sekine, A. Kasamatsu, T. Yoshida, S. Amakawa, and M. Fujishima, "A 32Gbit/s 16QAM CMOS receiver in 300GHz band," IEEE Int. Microw. Symp., pp.1703–1706, June 2017.
[12] S. Hara, K. Katayama, K. Takano, R. Dong, I. Watanabe, N. Sekine, A. Kasamatsu, T. Yoshida, S. Amakawa, and M. Fujishima, "A 32 Gbit/s CMOS receiver in 300GHz band," IEICE Trans. Electronics, vol.E101-C, no.7, pp.464–471, July 2018.
[13] S. Lee, S. Hara, T. Yoshida, S. Amakawa, R. Dong, A. Kasamatsu, J. Sato, and M. Fujishima, "An 80-Gb/s 300-GHz-band single-chip CMOS transceiver," IEEE J. Solid-State Circuits, vol.54, no.12, pp.3577–3588, Dec. 2019.
[14] S. Lee, S. Amakawa, T. Yoshida, Y. Morishita, Y. Kashino, S. Hara, and M. Fujishima, "300-GHz CMOS-Based wireless link using 40-dBi Cassegrain antenna for IEEE Standard 802.15.3d," IEEE Int. Symp. on Radio-Frequency Integrated Technology, pp.136–138, Sept. 2020.
[15] Y. Morishita, T. Teraoka, Y. Kashino, H. Asano, T. Sakamoto, N. Shirakata, K. Takinami, and K. Takahashi, "300-GHz-Band self-heterodyne wireless system for real-time bideo transmission toward 6G," IEEE Int. Symp. on Radio-Frequency Integrated Technology, pp.151–153, Sept. 2020.
[16] K. Matsumoto, Y. Chang, G.K. Tran, and K. Araki, "Frequency domain phase noise compensation employing adaptive algorithms for millimeter-wave OFDM systems," IEEE Asia-Pacific Microwave Conference, FR1G-35, pp.1262–1264 Nov. 2014.
[17] A.G. Armada, "Understanding the effects of phase noise in orthogonal frequency division multiplexing (OFDM)," IEEE Trans. on Broadcasting, vol.47, no.2, pp.153–159, June 2001.
[18] J.R. Pelliccio, H. Bachmann, and B.W. Myers, "Phase noise effects on OFDM wireless LAN performance," Applied Microwave & Wireless, pp.68–81, June 2001.
[19] Y. Morishita, T. Teraoka, Y. Kashino, H. Asano, T. Sakamoto, N. Shirakata, K. Takinami, and K. Takahashi, "Real-time video transmission with 300-GHz-Band OFDM wireless communication device," IEICE Technical Report, MW2019-64, pp.49–54, Sept. 2019.
[20] Y. Shoji, K. Hamaguchi, and H. Ogawa, "Millimeter-wave remote self-heterodyne system for extremely stable and low-cost broadband signal transmission," IEEE Trans. Microw. Theory Tech., vol.50, no.6, pp.1458–1468, June 2002.
[21] Y. Shoji and H. Ogawa, "70-GHz-band MMIC transceiver with integrated antenna diversity system: application of receiver-module-arrayed self-heterodyne technique," IEEE Trans. Microw. Theory Tech., vol.52, no.11, pp.2541–2549, Nov. 2004.
[22] S. Lee, R. Dong, S. Hara, K. Takano, S. Amakawa, T. Yoshida, and M. Fujishima, "A 6-mW-DC-power 300-GHz CMOS receiver for near-field wireless communications," IEEE Int. Microw. Symp., pp.504–507, June 2019.
[23] K. Takano, S. Amakawa, K. Katayama, S. Hara, T. Yoshida, and M. Fujishima, "300 GHz CMOS transmitter module for terahertz com-

municataion," IEICE Trans. Electron. (Japanese Edition), vol.J102-C, pp.348–355, Dec. 2019.
[24] S. Hara, K. Takano, K. Katayama, R. Dong, K. Mizuno, K. Takahashi, I. Watanabe, N. Sekine, A. Kasamatsu, T. Yoshida, S. Amakawa, and M. Fujishima, "300-GHz CMOS receiver module with WR-3.4 waveguide interface," Eur. Microw. Conf., pp.396–399, Sep. 2018.
[25] K. Takano, K. Katayama, S. Hara, R. Dong, K. Mizuno, K. Takahashi, A. Kasamatsu, T. Yoshida, S. Amakawa, and M. Fujishima, "300-GHz CMOS transmitter module with built-in waveguide transition on a multilayered glass epoxy PCB," IEEE Radio and Wireless Symp., pp.154–156, Jan. 2018.
[26] S. Amakawa and M. Fujishima, "300-GHz-band CMOS transmitter and receiver modules with WR-3.4 waveguide interface," IEEE Int. Microw. Conf. on Hardware and Systems for 5G and Beyond, pp.1–3, Aug. 2019.
[27] T. Tajima, H.-J. Song, and M. Yaita, "Design and analysis of LTC-C-integrated planar microstrip-to-waveguide transition at 300 GHz," IEEE Trans. Microw. Theory Tech., vol.64, no.1, pp.106–114, Jan. 2016.
[28] J. Sato, Y. Morishita, and Y. Kashino, "A study of manufacturing accuracy of 300 GHz band cassegrain antenna," Proc. Society Conf. IEICE, C-2-46, Sept. 2018.
[29] H. Sawada, A. Kanno.N. Yamamoto, K. Fujii, A. Kasamatsu, K. Ishizu, F. Kojima, H. Ogawa, and I. Hosako, "High gain antenna characteristics for 300 GHz band fixed wireless communication systems," Progress in Electromagnetics Research Symp., pp.1409–1412, Nov. 2017.
[30] P. Rodríguez-Vázquez, J. Grzyb, B. Heinemann, and U.R. Pfeiffer, "A 16-QAM 100-Gb/s 1-m wireless link with an EVM of 17% at 230 GHz in an SiGe technology," IEEE Microwave Wireless Compon. Lett., vol.29, no.4, pp.297–299, April 2019.

Yohei Morishita received the B.E. degree from SaitamaUniversity, Saitama, Japan, in 2005 and the M.E. and Ph.D. degrees from Tokyo Institute of Technology, Tokyo, Japan, in 2007 and 2014, respectively. In 2007, he joined Matsushita Electric Industrial (Panasonic) Co., Ltd., Japan. Since then he has been working on the research and development of analog and RF circuits for wireless communications. His research interests include digital-RF, mmW/THz technologies and IoT wireless network.

Sangyeop Lee received the B.E. degree in electrical and electronic engineering from the Tokyo Institute of Technology, Tokyo, Japan, in 2009, and the M.E. and Ph.D. degrees in electronics and applied physics from the Tokyo Institute of Technology, Yokohama, Japan, in 2010 and 2013, respectively. After working for a Korean Research Institute, Agency for Defense Development (ADD), Daejeon, South Korea, he joined Hiroshima University, Higashihiroshima, Japan, as a Researcher, in 2017, where he is currently an Assistant Professor. His current research interests include the design of millimeter-wave and terahertz CMOS circuits.

Toshihiro Teraoka received the B.S. and M.S. degrees in electrical engineering from Kyoto University, Kyoto, Japan, in 1993 and 1995, respectively. In 1995, he joined Panasonic Corporation, Yokohama, Japan, where he has been engaged in research and development on antennas and millimeter-wave circuitry.

Ruibing Dong received the B.E. degree from Hunan University in 2004, M.E. degree from South China University of Technology in 2008, and Ph.D. degree from Kyushu University in 2011. In 2015, he joined the National Institute of Information and Communication Technology (NICT), Koganei, Japan as a researcher. His research interests are millimeter wave and low-power CMOS circuits.

Yuichi Kashino received the B.S. and M.S. degrees in computer science and engineering from Nagoya Institute of Technology, Tokyo, Japan, in 2005 and 2007, respectively. In 2007, he joined Panasonic Mobile Communications R&D Lab. Co., Ltd., Japan, where he has been engaged in research and development of antenna on microwave and millimeter-wave.

Hitoshi Asano In 1991, he joined Matsushita Communication Sendai (Panasonic System Networks) R&D Lab. Co., Ltd., Sendai Japan. Since then, he has been engaged in the design of digital basebands for mobile communication systems, and has been working on the design of the development of LSIs and Communication devices. Since 2004, he has been engaged in research and development of millimeter-wave high-speed wireless communication systems and radar applications, and mainly promoted research and development of prototype equipment.

Shinsuke Hara received the B.E., M.E. and Ph.D. degrees in physics from the Tokyo University of Science in 2000, 2002 and 2006, respectively. In 2013, he joined the National Institute of Information and Communication Technology (NICT), Koganei, Japan as a Researcher. His research interests are millimeter wave CMOS circuits design and nano-scale semiconductor devices.

Kyoya Takano received the B.E., M.E. and Ph.D. degrees in Electrical Engineering from the University of Tokyo in 2006, 2008 and 2012, respectively. From 2012 to 2018, he was a project assistant professor with the Graduate School of Advanced Sciences of Matter, Hiroshima University. Since 2018, he has been an assistant professor with the Department of Electrical Engineering, Tokyo University of Science. His current research interests are millimeter-wave and terahertz technologies.

Kosuke Katayama received his B.E. and M.E. degrees in electronics engineering from Hosei University in 1997 and 1999, respectively. He received his Ph.D. degree in materials engineering from Hiroshima University in 2003. After working at an RF simulator company, he joined Hiroshima University as a researcher in 2010. He has been an assistant professor at Waseda University since 2017. He is a member of RISP, JSAP, IEICE and IEEE.

Takenori Sakamoto received the B.S. and M.S. degrees in electrical engineering from Kyushu University, Fukuoka, Japan, in 1999, and 2001, respectively. In 2001, he joined Matsushita Electric Industrial (Panasonic) Co., Ltd., Kanagawa, Japan. Since then he has been engaged in the design of digital processing circuits for wireless communications. He is currently involved in the design of baseband LSIs for millimeter wave transceiver.

Naganori Shirakata received B.E. and M.E. degrees in electronics engineering from Kyoto Institute of Technology, Japan in 1993 and 1995 respectively. He joined Panasonic Corporation, (former Matsushita Electric Industrial Co., Ltd.), Osaka in 1995, where he worked on baseband signal processing of OFDM and MIMO for WLANs, ultra low power radio and WBAN systems. From 2010, he worked on the development of the PHY system and circuit design for millimeter wave transceiver, and system design for millimeter wave access point and network. He currently leads model-based development for industrial IoT systems. He is a co-recipient of the Electrical Science and Engineering Promotion Awards (the OHM Technology Award) in 2015.

Koji Takinami received the B.S. and M.S. degrees in electrical engineering from Kyoto University, Kyoto, Japan, in 1995 and 1997, respectively, and the Ph.D. degree in physical electronics from Tokyo Institute of Technology, Tokyo, Japan, in 2013. In 1997, he joined Matsushita Electric Industrial (Panasonic) Co., Ltd., Osaka, Japan. Since then he has been engaged in the design of analog and RF circuits for wireless communications. From 2004 to 2006, he was a visiting scholar at the University of California, Los Angeles (UCLA), where he was involved in the architecture and circuit design of the high efficiency CMOS power amplifier. In 2006, he joined Panasonic Silicon Valley Lab, Cupertino, CA, where he worked on high efficiency transmitters and low phase-noise digital PLLs. In 2010, he relocated to Japan and currently leads the development of R&D projects toward the next generation V2X (vehicle-to-everything) and the industrial IoT solutions, ranging from sub-6GHz to millimeter-wave frequencies. He is a co-recipient of the APMC 2012 best paper award, the RFIT 2020 best paper award and the best invited paper award from IEICE Electronics Society in 2015. He was a member of the ISSCC Technical Program Committee from 2013 to 2015.

Kazuaki Takahashi received the B.E. and M.E. degrees in electrical and computer engineering, and the Ph.D. degree in electrical engineering from Yokohama National University, Yokohama, Japan, in 1986, 1988 and 2006, respectively. In 1988, he joined the Tokyo Research Laboratory, Matsushita Electric Industrial Co. Ltd., Kawasaki Japan, where he was engaged in research and development of monolithic microwave ICs, millimeter wave ICs and radio systems for mobile communication equipment. His current research interests include the development of multi-gigabit wireless system and high resolution sensor system in millimeter wave and terahertz bands, and low-power radio systems for IoT systems, especially for advanced V2X, smart city and smart manufacturing applications. He is also working on wireless standards in IEEE802.11, Wi-Fi Alliance, and ITU-R etc. He is the Director of Wireless Technologies, of Engineering Division, Industrial Solutions Company, Panasonic Corporation, Yokohama Japan. Dr. Takahashi is a member of the IEEE.

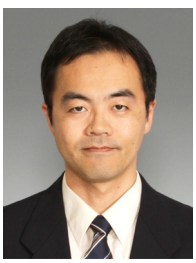

Akifumi Kasamatsu received his B.E., M.E. and Ph.D. degrees in electronics engineering from Sophia University, Tokyo, Japan, in 1991, 1993 and 1997, respectively. From 1997 to 1999, he was a research assistant at Sophia University. From 1999 to 2002, he was with Fujitsu Laboratories Ltd., Atsugi, Japan. Since 2002, he has joined National Institute of Information and Communications Technology (NICT), Koganei, Japan, where he is currently working as an executive researcher and a principal investigator of the terahertz wave electronics project. His current research interests are in wireless communication technology such as wireless transceivers and nano-scale semiconductor devices for millimeter wave and terahertz wave communications. Dr. Kasamatsu is a member of the Institute of Electronics, Information and Communication Engineers (IEICE) of Japan, and Japanese Society of Applied Physics (JSAP). He was awarded the 28th Meritorious Award on Radio presented by Association of Radio industries and Businesses of Japan, and the 2019 Maejima Hisoka Award presented by the Post and Telecom Association of Japan.

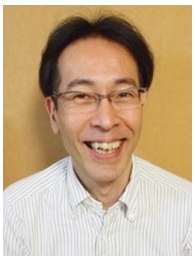

Takeshi Yoshida received the B.E., M.E. and Ph.D. degrees in engineering, all from Hiroshima University, Higashihiroshima, Japan, in 1994, 1996 and 2004, respectively. From 1996 to 2001, he was with the System Electronics Laboratories, Nippon Telegraph and Telephone Corporation, Atsugi, Japan. He is currently an Associate Professor at the Graduate School of Advanced Science and Engineering, Hiroshima University. He is a member of the Institute of Electrical and Electronics Engineers.

Shuhei Amakawa received the B.Eng., M.Eng., and Ph.D. degrees in engineering from The University of Tokyo, Tokyo, Japan, in 1995, 1997, and 2001, respectively, and the M.Phil. degree in physics from the University of Cambridge, Cambridge, U.K., in 2000. He was a Research Fellow with the Cavendish Laboratory, University of Cambridge from 2001 to 2004. After working for a couple of electronic design automation (EDA) companies, he joined the Integrated Research Institute, Tokyo Institute of Technology, Tokyo, in 2006. Since 2010, he has been with the Graduate School of Advanced Sciences of Matter, Hiroshima University, Higashihiroshima, Japan, where he is currently an Associate Professor. His research interests include modeling and simulation of nanoelectronic devices and systems, design of RF circuits and interconnects, and microwave theory and measurement. Dr. Amakawa has been serving as an Associate Editor for Electronics Letters since 2015.

Minoru Fujishima received the B.E., M.E. and Ph.D degrees in Electronics Engineering from the University of Tokyo, Japan in 1988, 1990 and 1993, respectively. He joined faculty of the University of Tokyo in 1988 as a research associate, and was an associate professor of the School of Frontier Sciences, University of Tokyo since 1999. He was a visiting professor at the ESAT-MICAS laboratory, Katholieke, Universiteit Leuven, Belgium, from 1998 to 2000. Since 2009, he has been a professor of the Graduate School of Advanced Sciences of Matter, Hiroshima University. He studied design and modeling of CMOS and BiCMOS circuits, nonlinear circuits, single-electron circuits, and quantum-computing circuits. His current research interests are in the designs of low-power millimeter- and short-millimeter-wave wireless CMOS circuits. He coauthored more than 50 journal papers and 120 conference papers. He served as a distinguished lecturer in IEEE solid-state circuits society from 2011 to 2012.